An Analysis of the Significance of the ^{14}N(n, p)^{14}C Reaction for Single-Event Upsets Induced by Thermal Neutrons in SRAMs

Andrea Coronetti, *Associate Member, IEEE*, Rubén García Alía, *Member, IEEE*, David Lucsanyi, Manon Letiche, Maria Kastriotou, Carlo Cazzaniga, Christopher D. Frost, *Member, IEEE*, and Frédéric Saigné

***Abstract*—The thermal neutron threat to the reliability of electronic devices caused by ^{10}B capture is a recognized issue that prompted changes in the manufacturing process of electronic devices with the aim of limiting as much as possible the presence of this isotope nearby device sensitive volumes (SVs). ^{14}N can also capture thermal neutrons and release low-energy protons (LEPs; through the ^{14}N(n, p)^{14}C reaction) that have high enough linear energy transfer (LET) to cause single-event upsets (SEUs). Typically, nitrogen is used in thin barrier layers made of TaN or TiN or even as insulator in the form of Si_3N_4. Numerical simulations on SVs calibrated on proton and ion experimental data and with an accurate description of the metallization layer on top of the sensitive region show that the presence of nitrogen in these thin barrier layers can be enough to justify the experimentally observed thermal neutron SEU cross section for a static random access memory (SRAM) sensitive to LEPs. Nevertheless, the expected SEU cross section from thermal neutrons is usually a few orders of magnitude lower than that of high-energy particles, therefore, not representing an important threat in atmospheric applications. At the same time, for high-energy accelerators, the contribution to the total soft error rate (SER) could become substantial, though easy to handle by margins.**

***Index Terms*—Boron, low-energy protons (LEPs), Monte Carlo simulations, nitrogen, single-event upset (SEU), static random access memory (SRAM), thermal neutrons.**

I. Introduction

THERMAL neutrons are an important contributor to any radiation environment where spallation reactions and neutron moderation are involved. This is the case of the atmosphere (ground level to flight altitudes) as well as of high-energy physics accelerators. Thermal neutrons can trigger single-event upsets (SEUs) in memory-based devices through indirect ionization following their nuclear absorption in ^{10}B atoms that may be present within or nearby sensitive cells, causing the release of an alpha and a Li ion. The ^{10}B(n, α)^{7}Li nuclear reaction is illustrated in Fig. 1.

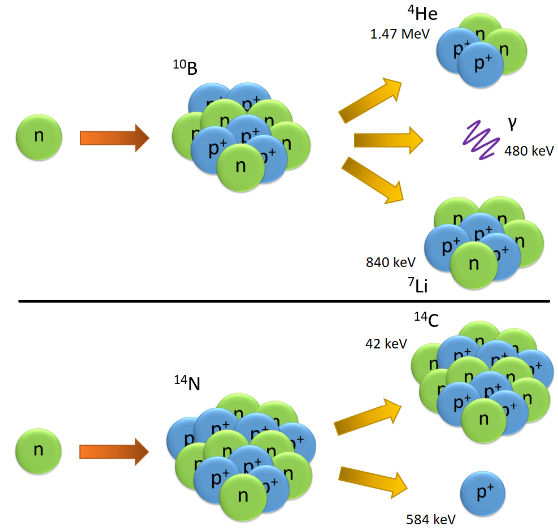

Fig. 1. Thermal neutron interaction with ^{10}B leading to the emission of an alpha particle and a Li ion as a result of nuclear capture (top) and with ^{14}N leading to the emission of a LEP as a result of neutron capture (bottom).

In the past [1], [2], [3], boron was employed in passivation layers for memory devices [borophosphosilicate glass (BPSG)]. Later, this process was abandoned. Nevertheless, boron is still used in semiconductor manufacturing in two other circumstances. In the first case, it is used as a dopant in p-type silicon. However, in this case, ^{10}B is filtered out from the implantation process by magnetic separation [4]. In the second case, it is used to reduce the resistance of the tungsten plugs [5] by deposition of B_2H_6, for which boron isotopic separation is not possible.

Several studies performed in the last decade [6], [7], [8], [9], [10], [11], [12], [13], [14] report thermal neutron sensitivity in bulk and FinFET static random access memories (SRAMs), flip-flops, and microcontrollers based on deep submicrometer technologies (<100 nm) and caused by the presence of boron nearby the sensitive cells of the various devices.

Manuscript received 14 October 2022; revised 17 December 2022 and 18 January 2023; accepted 20 January 2023. Date of publication 23 January 2023; date of current version 16 August 2023. This work was supported in part by the European Union's Horizon 2020 Research and Innovation Program through the Marie Sklodowska Curie Grant under Agreement 721624, in part by the European Union's Horizon 2020 Research and Innovation Program under Agreement 101008126, and in part by the French National Program "Investissements d'Avenir, IRT Nanoelec" under Grant ANR-10-AIRT-05.

Andrea Coronetti is with CERN, 1211 Geneva, Switzerland, and also with the Institute d'Électronique et des Systèmes, Université de Montpellier, 34090 Montpellier, France (e-mail: andrea.coronetti@cern.ch).

Rubén García Alía and David Lucsanyi are with CERN, 1211 Geneva, Switzerland.

Manon Letiche is with the Institute Laue-Langevin, 38000 Grenoble, France.

Maria Kastriotou, Carlo Cazzaniga, and Christopher D. Frost are with the Science and Technology Facilities Council, OX11 0QX Didcot, U.K.

Frédéric Saigné is with the Institute d'Électronique et des Systèmes, Université de Montpellier, 34090 Montpellier, France.

Color versions of one or more figures in this article are available at https://doi.org/10.1109/TNS.2023.3239407.

Digital Object Identifier 10.1109/TNS.2023.3239407

This work is licensed under a Creative Commons Attribution 4.0 License. For more information, see https://creativecommons.org/licenses/by/4.0/

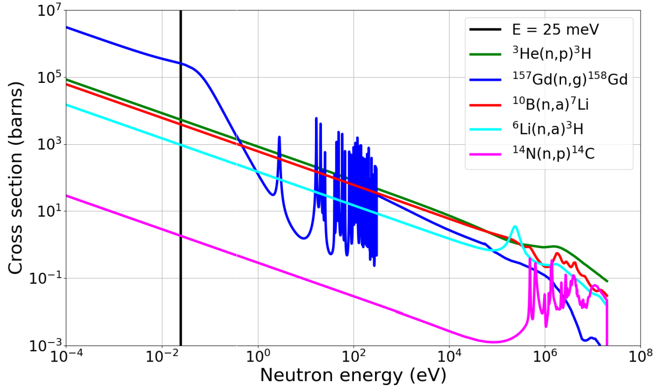

Fig. 2. Comparison among the capture cross sections of neutrons with ^{14}N, ^{10}B, ^{6}Li, ^{3}He, and ^{157}Gd as a function of the neutron energy [32].

As shown in Fig. 1, the nuclear reaction releases two light ions, an alpha particle and a Li ion. In 94% of the cases, the alpha is produced with an energy of 1.472 MeV and the Li ion with an energy of 840 keV, and also, a γ photon with an energy of 480 keV is emitted. In the remaining 6% of the cases, the alpha is generated with an energy of 1.776 MeV and the Li ion with an energy of 1014 keV, and no photon is generated. Depending on the sensitivity of the device, either one or both of the secondary ions can deposit enough energy in the sensitive volume (SV) to cause an upset.

In this article, the focus is shifted on another material commonly employed in the manufacturing of memory-based devices, i.e., nitrogen. Nitrogen is used in the back-end-of-line (BEOL) as either a thin barrier layer around the metal layers (typically, TiN and TaN are used) or as insulator (Si_3N_4). Therefore, given the state-of-the-art manufacturing technologies, much larger quantities of nitrogen (an actual constituent) can be expected in a memory device than of boron (more of a residual).

Nitrogen may be important, because thermal neutrons can be captured by ^{14}N atoms with the emission of a low-energy proton (LEP) with an energy of 584 keV (range in silicon of 7.46 μm [15]). This energy may further reduce as the proton travels through the BEOL, bringing the proton to enter the SV at an energy close to the Bragg peak (at around 50 keV) where the linear energy transfer (LET) is maximum. Therefore, given that many devices in the 28–90 nm sensitive node size have been shown in [16], [17], [18], [19], [20], [21], [22], [23], [24], [25], [26], [27], [28], [29], [30], and [31] to be very sensitive to LEPs, it is possible that they will also be significantly sensitive to thermal neutrons if nitrogen is used in their manufacturing process. Concerning the ^{14}N target nucleus, this turns into a ^{14}C product nucleus with an energy of just 42 keV, after the neutron capture and proton emission. Therefore, the isotope has insufficient range to reach the SV and become a hazard. This reaction is also shown in Fig. 1.

Despite the much larger abundance of nitrogen in a memory, the neutron capture cross section of ^{14}N is much lower than that of ^{10}B and of other isotopes, see Fig. 2, whose data were retrieved from the ENDF database [32]. For the thermal neutron energy, i.e., 25 meV, the ^{14}N capture cross section is as low as 1.8 barns (1 barn = 10^{-24} cm^2), whereas the ^{10}B cross section is about 3844 barns, therefore ≈2000 times larger.

In this work, experimental thermal neutron SEU measurements on an SRAM highly sensitive to LEPs [31] and Monte Carlo simulations embedding details of the construction analysis of the metallic and insulating overlayers seem to confirm that LEPs created through the ^{14}N(n, p)^{14}C reaction would indeed lead to upsets. In this respect, this article is further devoted to analyzing under which conditions nitrogen can become a threat as serious as that of boron for the soft error rate (SER) of a memory device in atmospheric and accelerator environments.

II. Experimental Measurements and Construction Analysis

The targeted device is the CY62167GE30-45ZXI, which is commercially available from Infineon. The memory is based on a 65-nm bulk technology and has a total capacity of 16 Mbits and a 3.3-V I/O voltage. It shall be noted that the commercial version has an embedded error correction code (ECC) that was disabled for the purpose of the various experimental SEU measurements. This memory has been characterized in a number of different radiation fields other than thermal neutrons [33], out of which the marked LEPs sensitivity stood out [31].

Thermal neutron testing was achieved at the ILL D50 facility [34]. Therefore, high fluxes of thermal neutrons (10^9 n/cm^2/s) are obtained by cooling down the fast neutrons emitted by the fission reactor (with a negligible fast neutron component, i.e., no SEUs were observed when covering the memory with 4 mm of B_4C to remove the thermal neutron component completely). The experimentally measured SEU cross section upon irradiation of 16 devices is $(4.76 \pm 0.78) \times 10^{-16}$ cm^2/bit. This SRAM was also tested with LEPs at CNA [31], [33], [35] with peak cross section $>10^{-9}$ cm^2/bit. Finally, to assess the relative impact of thermal neutrons in actual environments, it is necessary to relate the corresponding thermal neutron SER to that from high-energy neutrons (HENs). Therefore, one unit of this SRAM was also tested at ChipIr with atmospheric neutrons [36], with a resulting SEU cross section of $(1.16 \pm 0.24) \times 10^{-13}$ cm^2/bit. All error bars are calculated at 95% confidence level.

The structure of the BEOL of the memory was retrieved by means of scanning electron microscope (SEM) cross sectioning. Nitrogen was identified in thin barrier layers around copper and aluminum metal layers in TaN and TiN composites. In addition, some thin layers of Si_3N_4 were also identified in the passivation layer, which is placed the farthest from the SV. Although the actual configuration of the BEOL is not just monodimensional, it is still possible to summarize one-dimensionally its various layers, as listed in Table I.

Note that the SEM analysis did not provide an exact measurement for the thickness of the individual TaN and TiN layers, but these were combined with those of Cu and Al metal layers. This is the reason why, in the table, the data are left in

TABLE I

LIST OF MATERIALS PRESENT IN THE BEOL RESULTING FROM THE SEM ANALYSIS. THE SENSITIVE CELLS ARE PLACED AT THE BOTTOM OF THE STACK. THICKNESS OF METAL AND THIN BARRIER LAYERS WERE NOT GIVEN SEPARATELY. FOR THE PURPOSE OF THIS STUDY, THE THICKNESS OF THE TIN AND TAN THIN BARRIER LAYERS AS WELL AS THE METAL LAYERS IS LEFT IN PARAMETRIC FORMAT, THROUGH THE T PARAMETER

Name	Material(s)	Thickness [nm]
Passivation	Si_3N_4/SiO_2	360
TiNabove	TiN	1000 × T
Metal6	Al	1000 × (1-2T)
TiNbelow	TiN	1000 × T
Oxide5	SiO_2	960
TaN5above	TaN	980 × T
Metal5	Cu	980 × (1-2T)
TaN5below	TaN	980 × T
Oxide4	SiO_2	440
TaN4above	TaN	280 × T
Metal4	Cu	280 × (1-2T)
TaN4below	TaN	280 × T
Oxide3	SiO_2	280
TaN3above	TaN	170 × T
Metal3	Cu	170 × (1-2T)
TaN3below	TaN	170 × T
Oxide2	SiO_2	130
TaN2above	TaN	220 × T
Metal2	Cu	220 × (1-2T)
TaN2below	TaN	220 × T
Oxide1	SiO_2	100
TaN1above	TaN	150 × T
Metal1	Cu	150 × (1-2T)
TaN1below	TaN	150 × T
Plug	W	380
PolySi	Si	20

parametric format with a generic thickness parameter T that will be varied throughout the numerical analysis.

These thin barrier layers are placed at the top and at the bottom of each of these metal layers. In typical manufacturing processes, these thin barrier layers are obtained by depositing an amount of TaN or TiN in the order of 50–100 nm per 1 μm of metal. Therefore, as shown in the table, the thickness of these barrier layers is parametrized based on this ratio and on the overall thickness of the actual metal layer and its two thin barrier layers. For instance, taking the thin barrier layers to be 50-nm thick for 1 μm of metal, the resulting "TaN1above" and "TaN1below" layers in the table would be 7.5-nm thick and the "Metal1" layer 135-nm thick.

The SEM analysis did not reveal the presence of boron, and the manufacturer declares no boron is employed in the BEOL of the SRAM. Nevertheless, for the sake of the analysis, the presence of natural boron (80.1% ^{11}B and 19.9% ^{10}B) at the level of the tungsten plug will be considered with concentrations in the order of 10^{17}–10^{20} cm^{-3} [37].

III. NUMERICAL ANALYSIS FOR THIS DEVICE

A. Event-by-Event Scoring of LEPs

G4SEE [38] Monte Carlo simulations can be used to shed light on whether the measured experimental SEU cross section is due to LEPs emitted by thermal neutron interactions with nitrogen nuclei. The characteristics of the SV of this SRAM

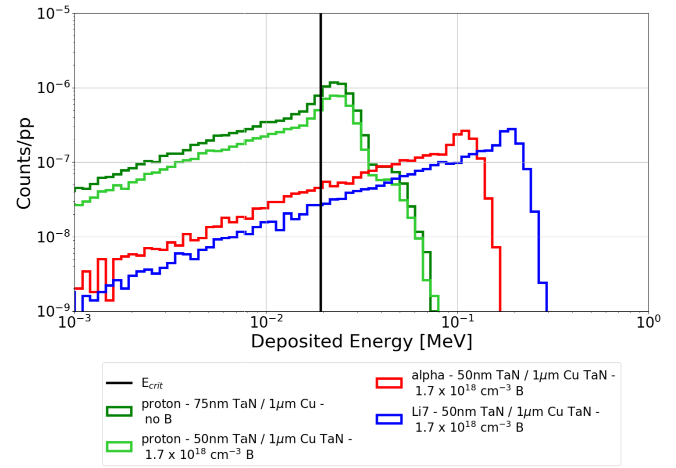

Fig. 3. Event-by-event scoring of energy deposition spectra by particle for the case: 1) with thin barrier TaN layers thickness of 75 nm per 1 μm of Cu and no B in the W plug and 2) with thin barrier TaN layers thickness of 50 nm per 1 μm of Cu and 1.7 × 10^{18} cm^{-3} natural B in the W plug. The critical energy required to cause an upset is also shown.

were determined in a previous study [31] based on the fitting of experimental proton and ion SEU data.

The SV model is based on a 360-nm cubic rectangular parallelepiped (RPP) with 0.86-fC critical charge (19.35-keV critical energy). With respect to the previous study, a more detailed BEOL structure, which includes all the materials as listed in Table I, was introduced in the simulation geometry.

Simulations are performed including various amounts of nitrogen, by acting on the thickness parameter T in the range of 25–100 nm per 1 μm of metal, and of boron, by acting on the boron concentration in tungsten.

Some first simulations were done to understand whether the LEPs generated by the nitrogen in the BEOL would lead to energy deposition events in the SV that could exceed the critical charge/energy of the memory. The energy deposition distribution for various amounts of nitrogen is also compared with those arising when dispersing boron in the tungsten.

Fig. 3 provides the event-by-event scoring deposited energy spectra of LEPs, alphas, and Li ions released by the nuclear reactions of 25-meV neutrons with the nitrogen and boron included in the simulation. The graph also shows which is the critical energy required to cause an SEU for this memory SV model. As the plot shows, LEP events can exceed the critical energy, and the amount of nitrogen does not significantly alter the spectra; i.e., only the counts per primary are reduced, but not the maximum deposited energies.

Alphas and Li ions can deposit higher levels of energy than the LEPs. The alpha peak occurs at an energy five times higher than for LEPs and the Li ion peak at an energy ten times higher.

As shown in Table II, given their low range, the LEPs reaching the SV mostly originate in the thin barrier layers that are the nearest to the SV. However, as proven by the "TaN5above" and "TaN5below" layers, a higher amount of nitrogen far from the SV can compensate for the longer distance to be covered to reach the SV. Energy deposition

TABLE II

ORIGINATING THIN BARRIER LAYERS OF THE LEPS REACHING THE SV AND OF THOSE DEPOSITING A SUFFICIENT ENERGY TO CAUSE AN UPSET. BOTH QUANTITIES ARE REPORTED WITH PERCENTAGES. SIMULATION FOR THE CASE WITH 75 nm OF TaN FOR 1 μm OF Cu

Layer	LEP reaching SV	LEP reaching SV and depositing E $>$ E$_{crit}$
Passivation	0.0%	0.0%
TiNabove	0.0%	0.0%
TiNbelow	0.2%	0.2%
TaN5above	7.2%	10.9%
TaN5below	9.5%	14.8%
TaN4above	4.3%	5.8%
TaN4below	5.8%	7.5%
TaN3above	5.5%	6.2%
TaN3below	6.5%	7.1%
TaN2above	11.0%	10.7%
TaN2below	15.6%	12.8%
TaN1above	14.3%	11.4%
TaN1below	20.1%	12.6%

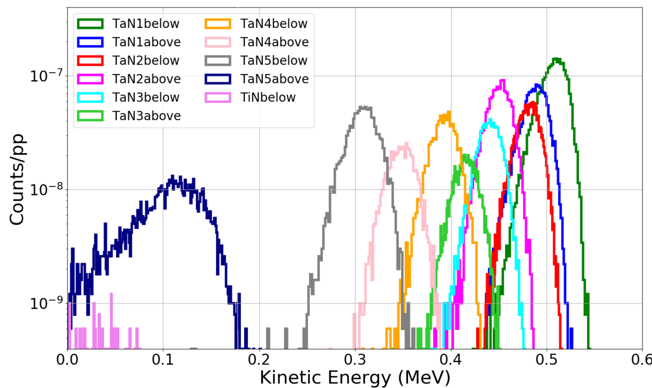

Fig. 4. Kinetic energy spectra of LEPs entering the SV based on the layer of origin in the BEOL. Simulation for the case with 75 nm of TaN per 1 μm of Cu.

events from LEPs exceeding the critical charge are almost equally distributed among the three closest and two farthest TaN thin barrier layers. This means that even if there are fewer LEPs coming from the farther layers, these LEPs arrive at the SV after having lost much more energy in the following BEOL layers and have, thus, higher LET. As it can be seen, no LEPs from “TiNabove” and “Passivation” layer make it to the SV due to the insufficient range.

To provide further insight about the characteristics of the LEPs as a function of the layer where they have originated, Fig. 4 displays the respective kinetic energy spectra of the LEPs. As expected, even for the closest layers to the SV, the spectrum is not monochromatic, but it spreads over some tens of keV. The spread increases the farther the point of origin is from the SV, but it is only for LEPs generated in the Tan5above layer that the energy spectra positions around the proton Bragg peak energy of 50 keV.

Fig. 5 shows the LET distributions of the LEPs reaching the SV as a function of the layer they are generated in. As the figure shows, the spread in terms of LET is quite small for the closest layers. The LET of all LEPs generated in all of the BEOL layers is almost always higher than

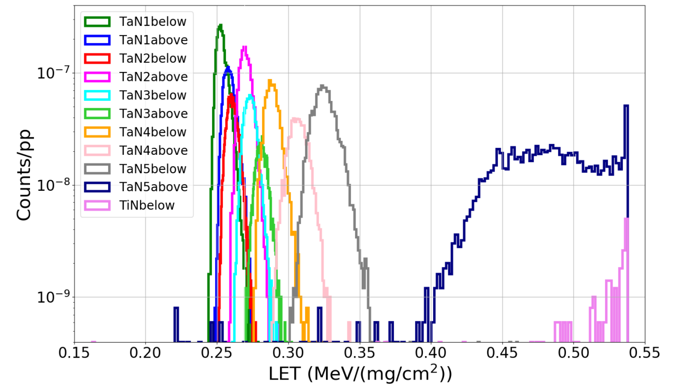

Fig. 5. LET spectra of LEPs entering the SV based on the layer of origin in the BEOL. Simulation for the case with 75 nm of TaN per 1 μm of Cu.

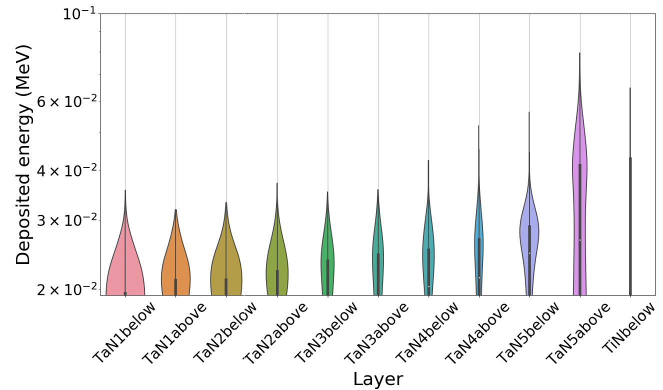

Fig. 6. Deposited energy distributions of LEPs in the SV based on the layer of origin in the BEOL. Simulation for the case with 75 nm of TaN per 1 μm of Cu. The lower bound of the y-axis is truncated at the level of E_{crit}.

0.25 MeV/(mg/cm^2), which is enough to cause an upset in this SRAM as seen with carbon ion testing [31], [33].

Finally, Fig. 6 depicts the energy deposition distributions of the LEPs based on the layer where the LEPs originated. The y-axis of the plot has been cut at the level of the critical energy of the SRAM at the bottom side to show only data relevant to the triggering of SEUs. Note that, in accordance with the LET, the LEPs generated in the closest layers typically deposit in the SV amount of energies that are just slightly above the critical energy and that never exceed it by more than a factor of 2. On the other hand, as the distance increases, the distribution widens, and the critical energy can be exceeded by even a factor of 4.

B. Nitrogen/Boron Required to Match the Experimental Thermal Neutron SEU Cross Section

The purpose of this section is to assess whether realistic amounts of nitrogen, as those previously defined, can lead to a sufficient amount of energy deposition events to justify the experimental thermal neutron SEU cross section or whether considering also the presence of boron would be required.

As previously mentioned, amounts of TaN (and TiN) in the thin barrier layers in the order of 50–100 nm per 1 μm of Cu (or Al) layer can be considered realistic. The analysis is, therefore, conducted by performing simulations with different

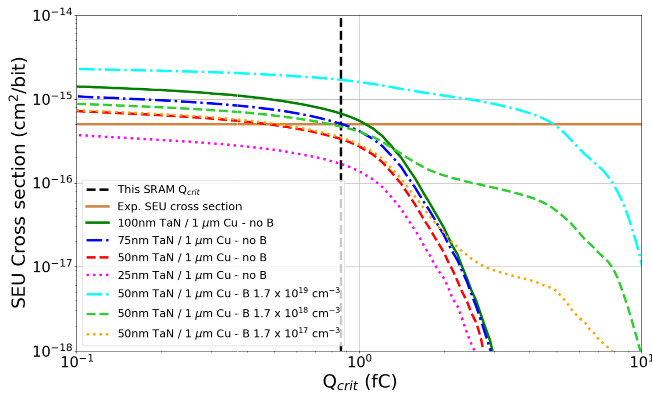

Fig. 7. Numerical SEU cross section as a function of the critical charge for various amounts of nitrogen in the BEOL and various boron concentrations in the tungsten plug. The plot also shows the critical charge of this SRAM SV model as well as the experimental thermal neutron SEU cross section to help identify the combinations of N and B matching this cross section.

values of the thickness parameter T, adapting accordingly the thickness of the thin barrier layers and of the metal layers. Simulations were performed using $T = 25$, 50, 75, and 100 nm per 1 μm of metal.

Fig. 7 depicts the SEU cross section as a function of the critical charge for these values of the T parameter. Two lines also mark the critical charge of this SRAM SV model and the experimental thermal neutron SEU cross section as guidance to understand whether realistic amounts of nitrogen would yield the experimentally observed cross section.

The figure shows that the case for $T = 75$ nm of TaN per 1 μm of Cu passes exactly through the intersection between the critical charge and the experimental cross section. This confirms that even small and realistic amounts of nitrogen in thin barrier layers are expected to contribute significantly to the thermal neutron cross section through the generation of LEPs.

It is also quite clear from the figure that there seems to be rather direct proportionality between the amount of TaN and the SEU cross section, given that the $T = 50$-nm case has a cross section twice as high as that of $T = 25$ nm and twice as low as that for $T = 100$ nm.

Even if it was possible to obtain an excellent match with nitrogen alone, for the sake of the discussion, it is also relevant to try to insert natural boron into the tungsten plug and to assess if the combination of nitrogen and boron could also provide a satisfactory match. In this case, of course, the simulations are run assuming a lower amount of TaN that matching the experimental cross section, i.e., with $T = 50$ nm.

The simulation data including natural boron are also reported in Fig. 7 alongside those without any boron. Three natural boron concentrations have been used: 1.7×10^{17}, 1.7×10^{18}, and 1.7×10^{19} cm^{-3}. The ^{10}B concentrations are just 19.9% of those of natural boron. The values of these concentrations have been chosen to find a good match for the experimentally measured thermal neutron SEU cross section in the case of $T = 50$ nm.

The figure shows that a uniform natural B concentration of 1.7×10^{18} cm^{-3}, coupled with $T = 50$ nm, also satisfies the experimentally measured thermal neutron SEU cross section. In this case, the contribution of LEPs from nitrogen to the total SEU cross section would be 71%, with just 29% due to the alphas and Li ions from boron.

Therefore, sticking at $T = 50$ nm, which is typically the minimum used in manufacturing processes, LEPs from nitrogen would still be the major contributor to the observed upsets, and even using a twice as lower amount ($T = 25$ nm) would result in at least 35% of the upsets coming from LEPs from nitrogen, i.e., not negligible.

A concentration of natural B of 1.7×10^{17} cm^{-3}, even if yielding more energetic energy deposition events, would provide negligible contribution to the overall SEU cross section. On the other hand, if the natural boron concentration is raised to 1.7×10^{19} cm^{-3}, then the events from nitrogen would be negligible, even when considering $T = 100$ nm. However, the SEU cross section would clearly become too large to match the experimental value. Therefore, it can be concluded that, if boron was present in this SRAM tungsten plug, its concentration would have to be limited to a few 10^{18} cm^{-3} or lower.

C. Nitrogen and Boron Relative Criticality

When nitrogen is present only in the thin barrier layers, which can indeed be very thin, it does not take a very high concentration of natural boron in the tungsten plug to make the impact of nitrogen completely negligible. As shown in Fig. 7, for a natural boron concentration of 1.7×10^{19} cm^{-3}, the SEU cross section is expected to grow by a factor of 3–10 at the considered critical charge with respect to the cross section that would result from the nitrogen in the thin barrier layers alone.

When considering lower critical charges, the gap reduces. At this natural boron concentration, the SEU cross section will, nevertheless, remain at least a factor of 2 higher than with nitrogen in the thin barrier layers alone. This natural boron concentration can be found quite often in tungsten plugs of commercial devices [37] and would typically result in SEU cross sections exceeding 10^{-15} cm^2/bit. Therefore, even relatively low concentrations of natural boron would, in general, make the impact of nitrogen in thin barrier layers negligible.

Among the materials that can be employed for semiconductor manufacturing, nitrogen can also be found in the form of silicon nitride (Si_3N_4). This material is used in the device under consideration in the top-level passivation layer of the BEOL. Due to the distance from the SV, this layer did not contribute at all to the SEU cross section because of the low range of the released protons that would just stop inside the BEOL.

Nevertheless, it may be possible to find, in some devices, much higher amounts of Si_3N_4 placed much closer to the SV, given that this material may be used, for instance, in place of SiO_2. In the context of this criticality analysis, it would, therefore, be interesting to verify what would be the SEU cross section if SiO_2 in the BEOL would be fully replaced by Si_3N_4.

Fig. 8 depicts the SEU cross section as a function of the critical charge for the cases in which SiO_2 and Si_3N_4 are

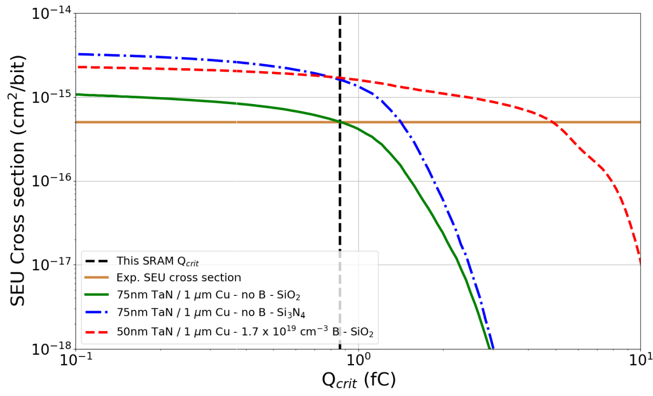

Fig. 8. Numerical SEU cross section as a function of the critical charge when SiO_2 is replaced with Si_3N_4, and no boron is considered in the tungsten plug. The results are compared with the case with the actual BEOL without boron and with a high boron concentration.

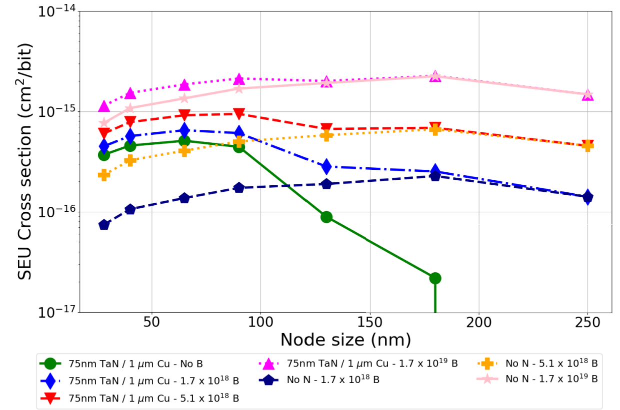

Fig. 9. Numerical SEU cross section as a function of the technology node for various amounts of nitrogen compounds and broron concentrations in the vicinity of the SV.

TABLE III
DATA USED TO SIMULATE THE THERMAL NEUTRON SEU CROSS SECTION FOR EACH TECHNOLOGY NODE

Node [nm]	22	40	65	90	130	180	250
SV size [nm]	255	310	360	420	480	560	625
Q_{crit} [fC]	0.4	0.6	0.86	1.3	2.3	3.4	8

contained in the BEOL with the same amount of TaN in the thin barrier layers ($T = 75$ nm). The results are also compared with a case with SiO_2 and high natural boron concentration (1.7×10^{19}).

Given that the total thickness of layers containing nitrogen has increased from 420 to 2690 nm, the SEU cross section has almost proportionally increased by a factor of 5 for the critical charge of this SRAM, reaching 1.62×10^{-15} cm^2/bit. The increase was such that it matched also the SEU cross section from the 1.7×10^{19} natural boron concentration case, becoming even slightly higher at lower critical charges. As it will be shown later, an SEU cross section this high would have important consequences for the hardness assurance in accelerator environments.

D. Analysis for Diverse Node Technologies

G4SEE simulations can also be performed to assess the relative importance of nitrogen and boron in contributing to the SEU cross section for technologies whose node varies from 22 to 250 nm. Since detailed models and construction analyses for devices in these nodes are not available down to the level of detail needed, this analysis is performed under some assumptions. For both the nitrogen content and placement, the BEOL used for the 65 nm SRAM under analysis will be retained. For the boron, the content will be varied, and its location will again be the tungsten plug, located in the same position as for the 65 nm SRAM. Therefore, no BPSG will be used in the simulations. This material typically characterized higher technology nodes than those considered here.

For the simulations, it is also necessary to define the SV size and critical charges characteristic of the technological nodes. For the critical charge, an extensive analysis for all the technology nodes of bulk silicon SRAMs is reported in the work from Kobayashi [39]. Multiple critical charges for the same node were evidenced in this work. Therefore, the critical charges that were adopted for the various nodes in this analysis, and reported in Table III, are interpolated from the values reported in that work. The critical charge for the 65-nm SRAM here reported (0.86 fC) is slightly lower with respect to other 65-nm examples reported by Kobayashi, but it aligns well with those of smaller nodes reported in that same work.

Concerning the SV size of the RPPs, a similar rescaling in terms of interpolation is applied, knowing that for a 250-nm SRAM, an SV size of 625 nm is suitable [40]. Then, intermediate nodes are rescaled based on this value and that for the 65-nm SRAM in this work, i.e., 360 nm. For the smaller nodes, a model for the 40 nm is available [31], and the 22 nm is rescaled accordingly. All data for the SV models used for the simulations are reported in Table III.

Fig. 9 depicts the numerical SEU cross sections as a function of the technology node size and as a function of the contents of nitrogen and boron. The trend obtained for the case without any boron points out that the presence of nitrogen becomes significant only for nodes below 100 nm. As the technology node increases, the nitrogen has a more and more negligible, and even null, effect on the SEU cross section.

Boron is expected to be dominant for the nodes above 100 nm starting from concentrations larger than 2×10^{18} cm^{-3}. In fact, for all the curves without nitrogen content, the SEU cross sections are seen to peak around 180 nm.

For lower technology nodes, the observations done for the 65 nm node still apply, although it is noted that the response due to the nitrogen peaks at around 65 nm and starts lowering for smaller nodes, probably because the shrinking of the SV is more impactful than the decrease in critical charge.

For cases in which both nitrogen and boron are considered, it is evident that the nitrogen provides a bump in the cross sections for nodes below 100 nm that becomes more and more negligible as the boron concentration increases.

IV. RADIATION ENVIRONMENTS OF CONCERN

Thermal neutrons can typically be found in radiation environments where fission or spallation reactions are involved.

TABLE IV

THERMAL NEUTRON FLUX, HEH_{eq} FLUX, AND R-FACTOR FOR VARIOUS TERRESTRIAL AND ACCELERATOR ENVIRONMENTS. ATMOSPHERIC DATA WERE RETRIEVED WITH THE MAIRE ONLINE TOOL [47] (FOR 51° LATITUDE AND 0° LONGITUDE). ACCELERATOR DATA WERE RETRIEVED WITH RADMON [48], [49] MEASUREMENTS

Environment	n_{th} flux [$cm^{-2}yr^{-1}$]	HEN/HEH_{eq} flux [$cm^{-2}yr^{-1}$]	R
Ground - 0 km	4.55×10^4	1.46×10^5	0.31
Avionics - 12 km	2.58×10^6	2.69×10^7	0.10
Lightly-shielded alcoves	1.54×10^9	1.60×10^8	9.60
Heavily-shielded alcoves	1.20×10^{10}	2.70×10^8	44.60

This is typically the case of nuclear power plants, high energy, and medical accelerators and of the terrestrial neutrons that can impact ground and avionics electronics.

In spite of the lower and lower reliance on natural boron in the manufacturing process of commercial devices, test standards for ground and atmospheric applications [41], [42] give high consideration to the thermal neutron hardness assurance. Thermal neutron sensitivity has also been an increasingly concerning issue for the hardness assurance of the electronics to be used in the high-energy accelerators [43], [44] involving both SRAM- and flash-based FPGAs and has brought to design specific guidelines for the design of systems that can be sensitive to them [45]. Similarly, for medical accelerators [46], thermal neutrons are considered the most significant threat to the reliability of the nearby electronics used to monitor the patient treatment.

Whereas most of these concerns pertain to the presence of boron close to the SV of the devices, the idea here is to assess whether the lower SEU cross section due to the presence of nitrogen may end up being a concern for these various environments.

The thermal neutron SER shall be put in relation to that arising from HENs ($E > 10$ MeV), in terrestrial environments, or high-energy hadron equivalents (HEH_{eq}, i.e., protons, neutrons, and pions whose $E > 20$ MeV and intermediate energy neutrons whose $E > 0.1$ MeV [50], [51]), in the accelerator environment, that are typically the main concern when it comes to SEEs. The R-factor is the ratio between the thermal neutron flux and that of higher energy particles in a certain environment.

Table IV reports the yearly thermal neutron and HEN (or HEH_{eq}) fluxes for two terrestrial cases at 0 and 12 km of altitude and for two CERN Large Hadron Collider cases with lightly shielded alcoves and heavily shielded alcoves. As the table shows, thermal neutron fluxes are expected to be more substantial when the amount of shielding (typically concrete, but it is also the case of the atmosphere) is increased. In the specific case of some of the considered CERN environment, in particular, the thermal neutron fluxes can be tens of times higher than those from HEH_{eq}.

SERs for this SRAM in the various environments can be obtained by multiplying the integral flux of thermal neutrons, and of high-energy particles, by the respective experimentally measured SEU cross section. Fig. 10 depicts the percentage contribution to the total SER of thermal neutrons and high-energy particles in the four environments under consideration (SiO_2 labeled data).

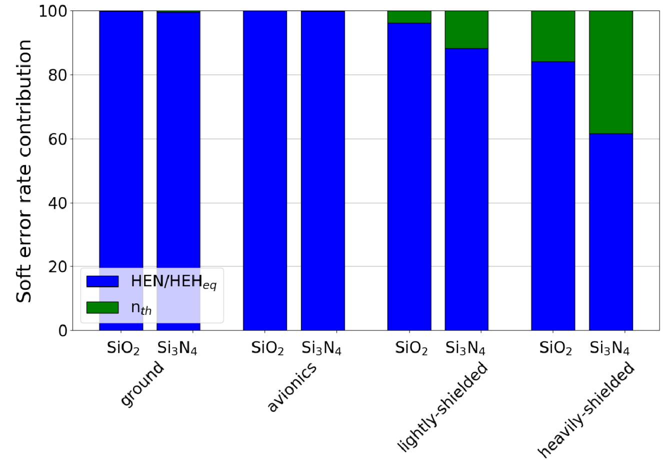

Fig. 10. Percentage contribution to the SER of thermal neutrons and high-energy particles for the four environments under consideration. Data calculated for the CY62167GE30-45ZXI from the experimental results (labeled SiO_2) and for the case in which Si_3N_4 is used in the BEOL in place of SiO_2 (labeled Si_3N_4).

As the bar plot shows, for this SRAM, the thermal neutrons are not expected to have a substantial impact on the atmospheric environments due to the fact that the HEN cross section is a factor of ≈200 higher than that of thermal neutron, and that the thermal neutron fluxes are lower than those from high-energy particles.

Concerning the accelerator, a more substantial effect is seen due to the relatively strong thermal neutron fluxes. For the lightly shielded alcoves, this contribution would anyway remain limited to <4%, whereas for the heavily shielded alcoves, this contribution would increase to 16%, a considerable contribution, though easy to margin.

Fig. 10 also depicts how these relative contributions would change if Si_3N_4 was used as a material in the BEOL in place of SiO_2 (Si_3N_4 labeled data). Therefore, in this case, the data rely on the numerically simulated SEU cross section for the thermal neutrons, whereas the experimental one is still used for high-energy particles.

No substantial contribution is expected in atmospheric environments considering that the thermal neutron SEU-cross section has incremented of less than a factor of 5. For the accelerator environments, the contribution to lightly shielded alcoves has increased to 12%, whereas that in heavily shielded alcoves has reached 38%. The latter would already provide a contribution that may bring a significant error in the SER estimation if thermal neutron characterization is neglected.

The situation may be more critical in medical accelerators where the flux of thermal neutrons can be a few million times higher than both the thermal and HEN fluxes at ground level [46], resulting in R-factors $>10^7$. In this case, even the tiny amount of nitrogen in the thin barrier layers will be sufficient to trigger SEUs in devices that would have, otherwise, not suffered any event from the HEN background.

This analysis allows concluding that thermal neutron sensitivity caused by the presence of nitrogen inside the BEOL of

a memory device would likely not be an issue for terrestrial applications, but that the potential hazard may be substantial for the high-energy physics and medical accelerator applications or whenever the *R*-factor exceeds 10.

V. Conclusion

This article introduces the possibility that thermal neutron SEUs may not only be caused by the interaction with ^{10}B in the proximity of the SV, but also by the interaction with ^{14}N that may result in the release of LEPs. The devices that may be affected are, therefore, only those showing a marked sensitivity to LEPs. At the same time, there is no need for a very large amount of nitrides (TaN, TiN, or Si_3N_4) to cause a substantial number of upsets in these kinds of devices.

The numerical simulations performed showed that it was possible to reproduce the experimentally measured thermal neutron SEU cross section without considering any boron in the BEOL of the SRAM and just based on realistic amounts (50–100 nm of TaN per 1 μm of copper) of nitrides. Nevertheless, the potential impact of both nitrogen and boron was also assessed in order to establish under which conditions boron SEUs would be dominant over nitrogen SEUs.

When Si_3N_4 is used in place of other insulators, the SEU cross section may grow quite proportionally to the amount of Si_3N_4 employed and can become more threatening.

The potential criticality of nitrogen induced SEUs was also assessed in the context of potential application environments of the commercial SRAM under consideration. The results show that an impact on terrestrial environments (i.e., ground and avionics) shall be disregarded. On the other hand, some substantial contributions were identified for heavily shielded areas in high-energy accelerators (and may also be applicable to some nuclear power plants and medical applications).

Acknowledgment

The authors would like to thank Robert C. Baumann for the insightful information about manufacturing practices and the useful discussion about the potential research lines. They would like to thank Helmut Puchner from Infineon, San Jose, CA, USA, for disclosing the information required to disable the embedded ECC in the CY62167GE30-45ZXI and on the boron usage in the manufacturing process of this SRAM. They would also like to thank the ILL, Grenoble, France, for the allocated beam time INDU-178 and INTER-499.

References

[1] R. C. Baumann and E. B. Smith, "Neutron-induced ^{10}B fission as a major source of soft errors in high density SRAMs," *Microelectron. Rel.*, vol. 41, no. 2, pp. 211–218, Feb. 2001.

[2] H. Kobayashi et al., "Soft errors in SRAM devices induced by high energy neutrons, thermal neutrons and alpha particles," in *IEDM Tech. Dig.*, San Francisco, CA, USA, Dec. 2002, pp. 337–340.

[3] A. Vazquez-Luque et al., "Neutron induced single event upset dependence on bias voltage for CMOS SRAM with BPSG," *IEEE Trans. Nucl. Sci.*, vol. 60, no. 6, pp. 4692–4696, Dec. 2013.

[4] T. Uemura et al., "Thermal-neutron SER mitigation by cobalt-contact in 7 nm bulk-FinFET technology," in *Proc. IEEE Int. Rel. Phys. Symp. (IRPS)*, Dallas, TX, USA, Mar. 2022, pp. 397–405.

[5] C.-H. Kim, I.-C. Rho, S.-H. Kim, Y.-S. Sohn, H.-S. Kang, and H.-J. Kim, "Improvement of adhesion performances of CVD-W films deposited on B_2H_6-based ALD-W nucleation layer," *Electrochem. Solid-State Lett.*, vol. 12, no. 3, p. H80, 2009.

[6] J. L. Autran, S. Serre, S. Semikh, D. Munteanu, G. Gasiot, and P. Roche, "Soft-error rate induced by thermal and low energy neutrons in 40 nm SRAMs," *IEEE Trans. Nucl. Sci.*, vol. 59, no. 6, pp. 2658–2665, Dec. 2012.

[7] T. Yamazaki et al., "Origin analysis of thermal neutron soft error rate at nanometer scale," *J. Vac. Sci. Technol. B, Nanotechnol. Microelectron., Mater., Process, Meas., Phenomena*, vol. 33, no. 2, Feb. 2015, Art. no. 020604.

[8] C. Weulersee et al., "Contribution of thermal neutrons to soft error rate," *IEEE Trans. Nucl. Sci.*, vol. 65, no. 8, pp. 1851–1857, Aug. 2018.

[9] Y.-P. Fang and A. S. Oates, "Thermal neutron-induced soft errors in advanced memory and logic devices," *IEEE Trans. Device Mater. Rel.*, vol. 14, no. 1, pp. 583–586, Mar. 2014.

[10] M. Cecchetto, R. G. Alía, S. Gerardin, M. Brugger, A. Infantino, and S. Danzeca, "Impact of thermal and intermediate energy neutrons on SRAM SEE rates in the LHC accelerator," *IEEE Trans. Nucl. Sci.*, vol. 65, no. 8, pp. 1800–1806, Aug. 2018.

[11] M. Cecchetto et al., "Thermal neutron-induced SEUs in the LHC accelerator environment," *IEEE Trans. Nucl. Sci.*, vol. 67, no. 7, pp. 1412–1420, Jul. 2020.

[12] E. C. Auden et al., "Thermal neutron-induced single-event upsets in microcontroller containing boron-10," *IEEE Trans. Nucl. Sci.*, vol. 67, no. 1, pp. 29–37, Jan. 2020.

[13] D. Oliveria et al., "High-energy versus thermal neutron contribution to processor and memory error rates," *IEEE Trans. Nucl. Sci.*, vol. 67, no. 6, pp. 1161–1168, Jun. 2020.

[14] H. Zhang et al., "Thermal neutron-induced soft-error rates for flip-flops designs in 16-nm bulk FinFET technology," in *Proc. IEEE Int. Rel. Phys. Symp.*, Monterrey, CA, USA, Apr. 2017, pp. 244–247.

[15] J. F. Ziegler and J. P. Biersack. *Stopping and Range of Ions in Matter*. Accessed: Aug. 2018. [Online]. Available: http://www.srim.org

[16] K. P. Rodbell, D. F. Heidel, H. H. K. Tang, M. S. Gordon, P. Oldiges, and C. E. Murray, "Low-energy proton-induced single-event-upsets in 65 nm node, silicon-on-insulator, latches and memory cells," *IEEE Trans. Nucl. Sci.*, vol. 54, no. 6, pp. 2474–2479, Dec. 2007.

[17] L. D. Edmonds and K. J. Edmonds, "A method for estimating SEU rates from protons by direct ionization," *IEEE Trans. Nucl. Sci.*, vol. 55, no. 5, pp. 2666–2678, Oct. 2008.

[18] D. F. Heidel et al., "Low energy proton single-event-upset test results on 65 nm SOI SRAM," *IEEE Trans. Nucl. Sci.*, vol. 55, no. 6, pp. 3394–3400, Dec. 2008.

[19] R. K. Lawrence, J. F. Ross, N. F. Haddad, R. A. Reed, and D. R. Albrecht, "Soft error sensitivities in 90 nm bulk CMOS SRAMs," in *Proc. IEEE Radiat. Effects Data Workshop*, Quebec City, QC, Canada, Jul. 2009, pp. 123–126.

[20] B. D. Sierawski et al., "Impact of low-energy proton induced upsets on test methods and rate predictions," *IEEE Trans. Nucl. Sci.*, vol. 56, no. 6, pp. 3085–3092, Dec. 2009.

[21] J. A. Pellish et al., "Impact of spacecraft shielding on direct ionization soft error rates for sub-130 nm technologies," *IEEE Trans. Nucl. Sci.*, vol. 57, no. 6, pp. 3183–3189, Dec. 2010.

[22] C. Weulersse, F. Miller, D. Alexandrescu, E. Schaefer, and R. Gaillard, "Assessment and comparison of the low energy proton sensitivity in 65 nm to 28 nm SRAM devices," in *Proc. 12th Eur. Conf. Radiat. Effects Compon. Syst.*, Seville, Spain, Sep. 2011, pp. 291–296.

[23] N. Seifert, B. Gill, J. A. Pellish, P. W. Marshall, and K. A. LaBel, "The susceptibility of 45 and 32 nm bulk CMOS latches to low-energy protons," *IEEE Trans. Nucl. Sci.*, vol. 58, no. 6, pp. 2711–2718, Dec. 2011.

[24] J. R. Schwank et al., "Hardness assurance testing for proton direct ionization effects," *IEEE Trans. Nucl. Sci.*, vol. 59, no. 4, pp. 1197–1202, Aug. 2012.

[25] J. A. Pellish et al., "Criticality of low-energy protons in single-event effects testing of highly-scaled technologies," *IEEE Trans. Nucl. Sci.*, vol. 61, no. 6, pp. 2896–2903, Dec. 2014.

[26] N. A. Dodds et al., "Hardness assurance for proton direct ionization-induced SEEs using a high-energy proton beam," *IEEE Trans. Nucl. Sci.*, vol. 61, no. 6, pp. 2904–2914, Dec. 2014.

[27] N. A. Dodds et al., "The contribution of low-energy protons to the total on-orbit SEU rate," *IEEE Trans. Nucl. Sci.*, vol. 62, no. 6, pp. 2440–2451, Dec. 2015.

[28] N. A. Dodds et al., "New insight gained on mechanisms of low-energy proton-induced SEUs by minimizing energy straggle," *IEEE Trans. Nucl. Sci.*, vol. 62, no. 6, pp. 2822–2829, Dec. 2015.

[29] J. Guillermin, N. Sukhaseum, P. Pourrouquet, N. Chatry, F. Bezerra, and R. Ecoffet, "Worst-case proton contribution to the direct ionization SEU rate," in *Proc. 17th Eur. Conf. Radiat. Effects Compon. Syst. (RADECS)*, Geneva, Switzerland, Oct. 2017, pp. 330–337.

[30] B. Ye et al., "Low energy proton induced single event upset in 65 nm DDR and QDR commercial SRAMs," *Nucl. Instr. Methods Phys. Res. B*, vol. 406, pp. 443–448, Sep. 2017.

[31] A. Coronetti et al., "Assessment of proton direct ionization for the radiation hardness assurance of deep sub-micron SRAMs used in space applications," *IEEE Trans. Nucl. Sci.*, vol. 68, no. 5, pp. 937–948, May 2021.

[32] National Nuclear Data Center. *Evaluated Nuclear Data File (ENDF)*. Accessed: Mar. 2022. [Online]. Available: https://www.nndc.bnl.gov/endf/

[33] A. Coronetti et al., "SEU characterization of commercial and custom-designed SRAMs based on 90-nm technology and below," in *Proc. IEEE Radiat. Effects Data Workshop Rec.*, Dec. 2020, pp. 56–63.

[34] J. Beaucour et al., "Grenoble large scale facilities for advanced characterisation of microelectronics devices," in *Proc. RADECS Conf.*, Sep. 2015, pp. 312–315.

[35] C. Cazzaniga et al., "Measurements of low-energy protons using a silicon detector for application to SEE testing," *IEEE Trans. Nucl. Sci.*, vol. 69, no. 3, pp. 485–490, Mar. 2022.

[36] A. Coronetti et al., "Thermal-to-high-energy neutron SEU characterization of commercial SRAMs," in *Proc. IEEE Radiat. Effects Data Workshop Rec.*, Jul. 2021, pp. 32–36.

[37] S.-J. Wen, S. Y. Pai, R. Wong, M. Romain, and N. Tam, "B10 finding and correlation to thermal neutron soft error rate sensitivity for SRAMs in the sub-micron technology," in *Proc. IEEE Int. Integr. Rel. Workshop Final Rep.*, South Lake Tahoe, CA, USA, Oct. 2010, pp. 31–33.

[38] D. Lucsanyi, R. G. Alia, K. Bilko, M. Cecchetto, S. Fiore, and E. Pirovano, "G4SEE: A Geant4-based single event effect simulation toolkit and its validation through monoenergetic neutron measurements," *IEEE Trans. Nucl. Sci.*, vol. 69, no. 3, pp. 273–281, Mar. 2022.

[39] D. Kobayashi, "Scaling trends of digital single-event effects: A survey of SEU and SET parameters and comparison with transistor performance," *IEEE Trans. Nucl. Sci.*, vol. 68, no. 2, pp. 124–148, Feb. 2021.

[40] R. G. Alia, "Radiation fields in high energy accelerators and their impact on single event effects," Ph.D. dissertation, Inst. D'Électronique Systèmes, Université de Montpellier, Montpellier, France, 2013.

[41] *Process Management for Avionics—Atmospheric Radiation Effects—Part 5: Assessment of Thermal Neutron Fluxes and Single Event Effects in Avionics Systems*, Standard IEC 62396-5, International Electrotechnical Commission (IEC), 2014.

[42] *Measurement and Reporting of Alpha Particle and Terrestrial Cosmic Ray Induced Soft Errors in Semiconductor Devices*, Standard JESD89B, Joint Electron Device Engineering Council (JEDEC), 2021.

[43] G. Tsiligiannis et al., "Radiation effects on deep submicrometer SRAM-based FPGAs under the CERN mixed-field radiation environment," *IEEE Trans. Nucl. Sci.*, vol. 65, no. 8, pp. 1511–1518, Aug. 2018.

[44] A. Scialdone, R. Ferraro, R. G. Alia, L. Sterpone, S. Danzeca, and A. Masi, "FPGA qualification and failure rate estimation methodology for LHC environments using benchmarks test circuits," *IEEE Trans. Nucl. Sci.*, vol. 69, no. 7, pp. 1633–1641, Jul. 2022.

[45] A. Zimmaro et al., "Testing and validation methodology for a radiation monitoring system for electronics in particle accelerators," *IEEE Trans. Nucl. Sci.*, vol. 69, no. 7, pp. 1642–1650, Jul. 2002.

[46] J. D. Wilkinson, C. Bounds, T. Brown, B. J. Gerbi, and J. Peltier, "Cancer-radiotherapy equipment as a cause of soft errors in electronic equipment," *IEEE Trans. Device Mater. Rel.*, vol. 5, no. 3, pp. 449–451, Sep. 2005.

[47] RadMod Research. *Models for Atmospheric Ionising Radiation Effects (MAIRE)*. Accessed: Aug. 2022. [Online]. Available: http://www.radmod.co.uk/maire

[48] D. Kramer et al., "LHC RadMon SRAM detectors used at different voltages to determine the thermal neutron to high energy hadron fluence ratio," *IEEE Trans. Nucl. Sci.*, vol. 58, no. 3, pp. 1117–1122, Jun. 2011.

[49] G. Spiezia et al., "A new RadMon version for the LHC and its injection lines," *IEEE Trans. Nucl. Sci.*, vol. 61, no. 6, pp. 3424–3431, Dec. 2014.

[50] K. Roed et al., "Method for measuring mixed field radiation levels relevant for SEEs at the LHC," *IEEE Trans. Nucl. Sci.*, vol. 59, no. 4, pp. 1040–1047, Aug. 2012.

[51] M. Cecchetto et al., "0.1–10 MeV neutron soft error rate in accelerator and atmospheric environments," *IEEE Trans. Nucl. Sci.*, vol. 68, no. 5, pp. 873–883, May 2021.